High gamma and beta band oscillations in left ventral posterior parietal cortex are regionally dissociated during verbal episodic encoding and recall

Rubinstein D[1], Camarillo-Rodriguez L[1], Waldman ZJ[1], Orosz I[5], Stein J[6], Das S[5], Gorniak R[3], Sharan AD[4], Gross R[10], Lega BC[11], Zaghloul K[12], Jobst BC[13], Davis KA[9], Wanda PA[8], Worrell G[14], Sperling MR[2], Weiss SA[1]

[1]Depts. of Neurology and Neuroscience,' [2]Dept. of Neurology, [3]Dept. of Radiology, [4]Dept. of Neurosurgery, Thomas Jefferson University, Philadelphia, PA, U.S.A. 19107. [6]Dept. of Neurology David Geffen School of Medicine at UCLA, Los Angeles, CA, U.S.A. 90095. [7]Penn Image Computing and Science Laboratory, Department of Radiology, [8]Department of Psychology, [9]Department of Neurology, University of Pennsylvania, Philadelphia, PA 19104, USA. [10]Department of Neurosurgery, Emory University, Atlanta GA, USA. [11]University of Texas Southwestern Medical Center, Department of Neurosurgery, Dallas TX, USA. 75390. [12]Surgical Neurology Branch, NINDS, NIH, Bethesda, MD 20892, USA. [13]Dartmouth-Hitchcock Medical Center, Department of Neurology, Lebanon NH, USA. 03756. [14]Depts. of Neurology, Physiology & biomedical Engineering, Mayo Clinic, Rochester, MN 55905.

Abstract (199)
The posterior parietal cortex (PPC) has a unique role in memory retrieval: fMRI[1–4] and electrocorticography[5] studies suggest that within the ventral PPC (VPC) specifically, there is an anterior-posterior functional divergence between externally-oriented and internally-oriented attention to memory (AtoM)[6–9]. However, the role of VPC during verbal episodic encoding, and the relationship between encoding- and retrieval-related activity, is less understood. Here we show that activation within a subregion of VPC is doubly dissociated between its anterior and posterior parts, during encoding compared to recall in a free recall task. We found that regional activation defined by increased high gamma power and decreased beta power oscillations during encoding and recall correlated with recall success. During word encoding, iEEG sites that showed this correlation were located anterior to those that showed deactivation. Conversely, during word recall, sites that showed stronger correlations between activity and number of words recalled were located more posteriorly. Our results demonstrate the significance of high gamma and beta oscillations suggesting a push-pull relationship between attention to external stimuli and internal memories within left ventral PPC. Knowledge of this divergence of function along the anterior-posterior axis within left ventral PPC may prove useful for guiding brain stimulation strategies.

Introduction (300)

Episodic memory is supported by diverse neural circuits and functions, including not only faithful information representation, but also attention to stimuli, during both encoding and subsequent recall. In contrast to spatial attention, which is confidently localized mostly to right parietal cortex[10], the neurophysiological correlates of attention to memory are less resolved. Recent evidence implicates left posterior parietal cortex, particularly ventral posterior parietal cortex (VPC) in attention to bottom-up, automatic memory retrieval[6–9,11]. For example, fMRI studies show decreased activation of VPC when new items are reliably differentiated from familiar ones, and patients with VPC lesions have difficulty specifically with uncued recall[1]. While these studies demonstrate the importance of VPC to attention to memory retrieval, its activation during encoding is less understood, often showing inconsistent responses[12].

Results (1354)

To test the hypothesis of a functional anterior-posterior gradient in VPC during verbal episodic encoding and recall, we utilized a verbal free recall task, performed by patients with epilepsy undergoing presurgical monitoring, with implanted subdural or depth macroelectrodes in Brodmann area (BA)40 left VPC (Fig. 1). In this task, patients were sequentially shown a list of words, and after an arithmetic distractor task were asked to recall as many as possible (Fig. 2A). The final data set consisted of 58 patients (Table. S1) with a total of 457 intracranial EEG (iEEG) task recordings from 322 unique depth and subdural electrode sites in left VPC, specifically from BA40 (Fig. 1), and the supramarginal gyrus.

We first asked whether activity in left BA40 was responsive to task stimuli, regardless of subsequent recall. Due to buffering constraints, we computed time-frequency (TF) representations of high gamma and beta power from 0.3s before, to 1.7s after word presentation. We then used a two-step approach to find significant stimulus-induced responses. First, we searched for regions in the TF plot containing large power modulations (>2 SD relative to pre-stimulus), and then used non-parametric cluster-based tests to test the significance of power modulations within this region, compared to the memory-unrelated distractor task. We identified significant (cluster-based Monte Carlo estimate, $p<0.05$) stimulus-induced high gamma (Fig. 2B,D, S1) and beta band (Fig. 2C,E,S1) responses in 34% (162/475) and 39% (183/475) of recordings, respectively, and in 79% (46/58) and 74% (43/58) of patients, respectively (Fig. 1). In 21% (98/457) of recordings and in 66% (38/58) of patients there was both a high gamma and beta band response. At the single trial level, positive responses were observable as distinct bursts of oscillatory power, and negative responses were observable as periods lacking oscillatory bursts (Fig. S5-S6). High gamma responses were approximately evenly split between stimulus-induced increases and decreases (88 and 90, respectively) as were beta band responses (116 and 120, respectively). This demonstrated the existence of neural populations in left BA40 that reliably activate (or deactivate) in response to visual word presentation.

We also examined high gamma and beta induced responses in left BA21 *i.e.* middle temporal gyrus (Fig. S2), left entorhinal cortex (BA28/34) (Fig. S3), and right BA40 (Fig. S4)(Table. S2). In left entorhinal cortex, high gamma and beta band responses were found in fewer patients (27% and 30%, respectively) and there was a reduction in absolute mean magnitudes of positive high gamma ($t(117)=-2.32$, $p<0.05$) and negative beta responses ($t(144)=-2.63$, $p<0.01$), compared to left BA40 (Fig. S1, S3). In right BA40 we found a reduced proportion of high gamma band responses (in 50% of patients). These negative high gamma responses in right BA40 were significantly decreased in absolute mean magnitudes ($t(164)=-4.58$, $p<0.001$) and increased in latency ($t(164)=5.54$, $p<0.001$)). However, we found a similar proportion of beta band responses (in 71% of patients) as in left BA40, but absolute mean magnitudes of negative beta band responses in right BA40 were significantly reduced ($t(201)=-2.49$, $p<0.05$) (Fig. S1,S4). In left BA21 we found similar proportions of high gamma and beta

band responses as in left BA40, but notably negative high gamma responses in left BA21 were increased in latency ($t(169)=3.63$, $p<0.001$), duration ($t(169)=10.7$, $p<0.001$) and absolute mean magnitudes ($t(169)=3.66$, $p<0.001$). Furthermore, the positive beta band responses in left BA21 were also increased in duration ($t(172)=2.47$, $p<0.05$) and absolute mean magnitudes ($t(172)=3.24$, $p<0.005$). The characteristics of induced responses in left BA40 were thus often distinct from responses in other regions (Fig. S1, S2).

We next asked if these stimulus-induced responses during encoding were modulated in magnitude by the success of subsequent recall. We thus tested for differences in oscillatory power within the same restricted region of the TF plot, between recalled and forgotten words (*i.e.* subsequent memory effect [SME]). We found that in 17% of the recordings that showed a significant high gamma response (27/162) from 11 patients, there was also significant SME ($p<0.05$, Fig. 2B,2D). In 9% of the recordings that showed a significant beta response (17/183) from 12 patients, there was a significant SME ($p<0.05$, Fig. 2C,E). These results indicated that indeed stimulus-induced responses were sometimes stronger for subsequently recalled words. We also examined the SME in left BA21 (Fig S2C), left entorhinal cortex (Fig S3C), and right BA40 (Fig S4C). Compared to left BA40, in right BA40 we found a reduced proportion of recordings showing an SME in high gamma (2% vs. 6% of all) and in fewer subjects (14% vs. 19%). Equivalent proportions showed a beta band SME (Fig S4A). Compared to left BA40, in left BA21 we found a reduced proportion of electrodes showing a high gamma SME (3% vs. 6%) but in the same proportion of patients (19%, Fig S2A). In beta band, we found the same proportion of electrodes showing an SME, but in a greater proportion of patients (28% vs. 21%) (Fig S2A). In left entorhinal cortex there were reduced proportions of recordings showing an SME in both high gamma (5% vs. 6%) and beta bands (1% vs. 4%) compared to left BA40 (Fig S3A).

To more directly test whether single-trial high gamma and beta oscillations during encoding could predict recall success, we performed logistic regression classification on the same set of patients in which an SME was observed. Using this approach, we were able to successfully predict recall success in 18 patients and 22 patient-task pairs (Table. S3) in which either a high gamma or beta band SME was observed, as assessed by area under ROC curve (AUROC) (AUROC range 0.56-0.76; mean 0.65±.06; $p<1e-9$, Fig 2F). In right BA40, recall success was predicted in 9 patients, with an AUROC range of 0.54-0.71 (0.62±.06) (Fig S4D). In left BA21, recall was predicted in 16 patients, and the AUROCs ranged from 0.51-0.73 (0.60±.07) (Fig S2D). In left entorhinal cortex, recall was predicted in 4 patients, and the AUROCs ranged from 0.61-0.68 (0.64±.03)(Fig S3D).

High gamma and beta oscillatory modulations in left BA40 during recall predict recall success

We next examined the role of left BA40 activity in memory retrieval. Specifically, we asked if high gamma or beta band power during the recall period was greater in the list-learning blocks where more words were correctly recalled. We first calculated high gamma and beta band power over the entire recall phase, normalized across session. We then tested for linear correlations between band power and recall number on a block-by-block level.

We found that in 10% (44/457) of recordings, the normalized or raw (Fig. S9) high gamma (n=28) and beta power (n=19) during recall correlated significantly with number of words recalled (FDR-corrected $p<.05$). Almost all correlations were positive for high gamma (26/28, Fig 3A), and negative for beta (15/19, Fig. 3A). In these electrodes we found that the high gamma and beta responses were often anti-correlated (Fig. S7). We also assessed the significance of the correlation of recall number and band-power through random permutations of recall number (n=1000) (Fig. S8).

Modulation of high-gamma and beta during encoding and recall are doubly dissociated along the anterior-posterior axis of left BA40

We first tested the hypothesis that recording sites showing positive stimulus-induced responses would be spatially divergent from those showing negative responses during encoding. Of the 162 recordings that exhibited stimulus-induced high gamma responses, we identified 136 unique electrode site/response type combinations. Electrode sites exhibiting positive high gamma responses were significantly more anterior to those exhibiting negative high gamma responses (mean neuroanatomical y-coord.: -37.9±10.6 vs. -45.4±9.5, CI: 4.1-10.9, $t(134)=4.36$, $p<.001$)(Fig 4A). We next asked if during the recall epoch more posterior VPC sites would exhibit a stronger correlation between high-gamma power and the number of words recalled. We found a significant correlation between R2 associated with the high-gamma recall correlation, and the y-coordinate ($r(27)=-.46$, $p<.05$)(Fig 4B).

We then performed the same analysis in beta band, hypothesizing that we would see the same effect, but reversed in polarity. As hypothesized, electrode sites exhibiting negative beta band responses were significantly more anterior to those exhibiting positive beta band responses (mean neuroanatomical y-coord.: -38.8±10.3 vs. -43.4±9.8, CI: 1.4-7.8, $t(157)=2.86$, $p<.005$)(Fig 4A), and we found a significant negative correlation between R2 associated with the recall correlation, and the y-coordinate ($r(18)=-.50$, $p<.05$)(Fig 4B).

Discussion (204)

In summary, high gamma and beta oscillations in the left VPC exhibit clear SMEs that can be utilized to predict verbal episodic memory performance during both encoding and recall. While other brain regions such as the left middle temporal gyrus also demonstrated high-gamma and beta SMEs in this study and in prior work[13–15], the left VPC SME's are particularly intriguing because the left VPC has been implicated in mediating attention to memory[6–9,11]. In the prefrontal cortex of primates anti-correlated high-gamma and beta oscillations may serve as an attractor state to encode working memory trace during the encoding, storage and retrieval phases[16,17]. It is unclear if the high-gamma and beta oscillations in the left VPC similarly represent a memory trace, attention to memory, or perhaps semantic or phonetic processing[2,18,19] important in both attention and memory. In the context of these oscillations mediating attention, prior fMRI and electrocorticography (ECoG) studies have also shown that an anterior-posterior gradient in the VPC may function to regulate attention to the environment and attention to memory in a push-pull manner[5,7–9]. To better differentiate whether high-gamma and beta oscillations in the left VPC mediate memory and/or attention future investigations could utilize cued and non-cued recall design[1], and also utilize information encoding measures[16,17].

Acknowledgements

We thank Blackrock Microsystems for providing neural recording and stimulation equipment. This work was supported by the DARPA Restoring Active Memory (RAM) program (Cooperative Agreement N66001-14-2-4032). The views, opinions, and/or findings contained in this material are those of the authors and should not be interpreted as representing the official views or policies of the Department of Defense or the U.S. Government. Dr. Weiss is supported by 1K23NS094633-01A1. Dr. Jobst was funded by this grant NSF EPSCoR "Neural Bases of Attention" OIA-1632738

Conflicts of Interest

S.A.W. and Z.J.W. both hold more than 5% equity interest in Fastwave L.L.C., an EEG software manufacturer.

References

1. Ciaramelli, E., Grady, C., Levine, B., Ween, J. & Moscovitch, M. Top-down and bottom-up attention to memory are dissociated in posterior parietal cortex: neuroimagingand and neuropsychological evidence. *J. Neurosci. Off. J. Soc. Neurosci.* **30**, 4943–4956 (2010).
2. Humphreys, G. F. & Lambon Ralph, M. A. Fusion and Fission of Cognitive Functions in the Human Parietal Cortex. *Cereb. Cortex N. Y. N 1991* **25**, 3547–3560 (2015).
3. Uncapher, M. R. & Wagner, A. D. Posterior parietal cortex and episodic encoding: insights from fMRI subsequent memory effects and dual-attention theory. *Neurobiol. Learn. Mem.* **91**, 139–154 (2009).
4. Nelson, S. M. *et al.* A parcellation scheme for human left lateral parietal cortex. *Neuron* **67**, 156–170 (2010).
5. Gonzalez, A. *et al.* Electrocorticography reveals the temporal dynamics of posterior parietal cortical activity during recognition memory decisions. *Proc. Natl. Acad. Sci. U. S. A.* **112**, 11066–11071 (2015).
6. Cabeza, R., Ciaramelli, E., Olson, I. R. & Moscovitch, M. The parietal cortex and episodic memory: an attentional account. *Nat. Rev. Neurosci.* **9**, 613–625 (2008).
7. Hutchinson, J. B. *et al.* Functional heterogeneity in posterior parietal cortex across attention and episodic memory retrieval. *Cereb. Cortex N. Y. N 1991* **24**, 49–66 (2014).
8. Sestieri, C., Corbetta, M., Romani, G. L. & Shulman, G. L. Episodic memory retrieval, parietal cortex, and the default mode network: functional and topographic analyses. *J. Neurosci. Off. J. Soc. Neurosci.* **31**, 4407–4420 (2011).
9. Sestieri, C., Shulman, G. L. & Corbetta, M. The contribution of the human posterior parietal cortex to episodic memory. *Nat. Rev. Neurosci.* **18**, 183–192 (2017).
10. Corbetta, M. & Shulman, G. L. SPATIAL NEGLECT AND ATTENTION NETWORKS. *Annu. Rev. Neurosci.* **34**, 569–599 (2011).

11. Ciaramelli, E., Grady, C., Levine, B., Ween, J. & Moscovitch, M. Top-down and bottom-up attention to memory are dissociated in posterior parietal cortex: neuroimagingand and neuropsychological evidence. *J. Neurosci. Off. J. Soc. Neurosci.* **30**, 4943–4956 (2010).
12. Uncapher, M. R. & Wagner, A. D. Posterior parietal cortex and episodic encoding: insights from fMRI subsequent memory effects and dual-attention theory. *Neurobiol. Learn. Mem.* **91**, 139–154 (2009).
13. Ezzyat, Y. *et al.* Closed-loop stimulation of temporal cortex rescues functional networks and improves memory. *Nat. Commun.* **9**, 365 (2018).
14. Kucewicz, M. T. *et al.* Evidence for verbal memory enhancement with electrical brain stimulation in the lateral temporal cortex. *Brain J. Neurol.* **141**, 971–978 (2018).
15. Kragel, J. E. *et al.* Similar patterns of neural activity predict memory function during encoding and retrieval. *NeuroImage* **155**, 60–71 (2017).
16. Lundqvist, M. *et al.* Gamma and Beta Bursts Underlie Working Memory. *Neuron* **90**, 152–164 (2016).
17. Lundqvist, M., Herman, P., Warden, M. R., Brincat, S. L. & Miller, E. K. Gamma and beta bursts during working memory readout suggest roles in its volitional control. *Nat. Commun.* **9**, 394 (2018).
18. Binder, J. R., Desai, R. H., Graves, W. W. & Conant, L. L. Where is the semantic system? A critical review and meta-analysis of 120 functional neuroimaging studies. *Cereb. Cortex N. Y. N 1991* **19**, 2767–2796 (2009).
19. Price, C. J. A review and synthesis of the first 20 years of PET and fMRI studies of heard speech, spoken language and reading. *NeuroImage* **62**, 816–847 (2012).

20. Oostenveld, R., Fries, P., Maris, E. & Schoffelen, J.-M. FieldTrip: Open source software for advanced analysis of MEG, EEG, and invasive electrophysiological data. *Comput. Intell. Neurosci.* **2011**, 156869 (2011).
21. Maris, E. & Oostenveld, R. Nonparametric statistical testing of EEG- and MEG-data. *J. Neurosci. Methods* **164**, 177–190 (2007).
22. Hochberg, Y. & Benjamini, Y. More powerful procedures for multiple significance testing. *Stat. Med.* **9**, 811–818 (1990).
23. Avants, B. B., Epstein, C. L., Grossman, M. & Gee, J. C. Symmetric diffeomorphic image registration with cross-correlation: evaluating automated labeling of elderly and neurodegenerative brain. *Med. Image Anal.* **12**, 26–41 (2008).

Methods

Task

A verbal free recall task was administered as part of the Defense Advanced Research Projects Agency (DARPA) Restoring Active Memory (RAM) project, to which patients consented during pre-surgical epileptic monitoring. The task consisted of 12 words displayed sequentially over 30s, followed by a 20s arithmetic distractor task, ending with a 30s recall period (Fig 2a)[13–15]. This block was repeated 25 times per session. In one task variant, words were selected randomly from a list of nouns; in a second variant, 3 categories were used to draw 4 words each, from a possible 25 semantic categories (http://memory.psych.upenn.edu/Word_Pools). Data were collected across sites including: Thomas Jefferson University Hospital (Philadelphia, PA), Mayo Clinic (Rochester, MN), Hospital of the University of Pennsylvania (Philadelphia, PA), Dartmouth-Hitchcock Medical Center (Lebanon, NH), Emory University Hospital (Atlanta, GA), National Institutes of Health (Bethesda, MD), University of Texas Southwestern Medical Center (Dallas, TX), and Columbia University Medical Center (New York, NY).

Recordings

Intracranial recordings were from depth, grid, and strip electrodes (AdTech Inc., PMT Inc.) implanted based on patient-specific needs. Recordings were collected with Nihon Kohden® EEG-1200, Natus XLTek® EMU 128, or Grass® Aura-LTM64 systems, depending on the site of data collection. Sampling rates ranged from 500-2000Hz depending on site. Data were referenced to common intracranial, scalp, or mastoid contacts. Bipolar montages were calculated from subtracting adjacent electrodes, and served as the electrodes used in this analysis. Bipolar electrode data were visually inspected for epileptic activity, low signal-to-noise, and artifact, and removed from analyses accordingly. Out of a pool of 314 patients, 119 had depth or subdural electrodes placed in left Brodmann area 40, our region of interest, as defined in standard Talairach space (www.talairach.org). Of these 119 patients, a final set of 58 were selected, with 322 electrode sites that were not contaminated with noise and not located in seizure onset or irritative zones, and which comprised 457 unique electrode-task recordings (Fig 1).

Stimulus-Induced Response Wavelet-based time-frequency representations.

We tested for significant word-induced responses using non-parametric cluster-based tests in FieldTrip[20] comparing encoding to distractor epochs, separately for each electrode-task recording[21]. To limit the scope of the test, we first searched for power modulations of at least two standard deviations lasting at least 50ms, in the 1.5s following word presentation compared to the 300ms prestimulus period, in the mean power across sessions. The frequency- and time-span of these modulations defined a region of interest in time-frequency space. The cluster-based tests comparing encoding to distractor epochs were performed within this region of interest, using alpha=0.1 to define the initial cluster, and alpha=0.025 (0.05 for 2-sided test) as the significance threshold. Monte-Carlo estimates of p values were calculated.

Subsequent Memory Effects

We tested for differences in oscillatory power during encoding between recalled and forgotten words (a.k.a. subsequent memory effect [SME]), but restricted to the recordings that showed a significant induced response, and further restricted to the same region of TF space in which the induced response was found. The non-parametric cluster-based statistical tests used for this comparison were identical to those used for the previous tests, comparing encoding and distractor epochs.

We tested the ability of single trial high gamma and beta power modulations to predict recall success using the following approach: for each patient with a recording showing a significant SME, we implemented logistic regression classification using all recordings from the same patient that showed significant induced responses during encoding. As classification features, we used mean high gamma and beta power over the region in time-frequency space that showed either the significant SME, or the greatest induced response if there was no SME. These features were constructed independently for each recording, and independently for high gamma and beta band. Matlab ('fitglm' function) was used to generate the logistic regression model using the first half of the patient's data, and applied to the second half to generate predictions. Classification performance was assessed using area under ROC curves (AUROC).

Correlations with Recall-Epoch Power

Linear correlation were tested between high gamma and beta power during the recall epoch, and the number of words recalled during that period. Specifically, for each complete session there were 25 data points corresponding to the 25 blocks, and the 25 recall periods that occur at the end of each block. Since there were 12 words per block, recall number ranged from 0 to 12. High gamma and beta band power was calculated across the entire 30 second recall period using the 'bandpower' function in Matlab, and normalized by session, by subtracting the mean and standard deviation of session-wide band-power from each block in a given session. This session-normalized value was input into a linear regression model, along with recall number, to calculate the relationship between high gamma power and recall number. Multiple comparisons correction was performed using a false discovery rate algorithm on the resulting p values on a subject-level basis. FDR[22] was also assessed using permutation tests: for each task recording, recall number was randomly permuted across blocks, and the correlation with band power was recalculated. This was performed 1000 times, yielding 1000 separate distributions of correlation values and associated p values.

Spatial Analysis

Prior to electrode implantation T1-weighted MRIs were obtained for each individual. Post-implantation CT scans were co-registered with the pre-implantation MRIs using ANTS with neuroradiologist supervision. These images were then transformed into standard MNI and

Talairach coordinates in order to identify the electrode coordinates in standard space[13,14,23]. Brodmann areas were additionally identified for each electrode contact, based on these localizations. Only electrode contacts from left BA40 were used in this study, although an alternative atlas based segmentation indicated that a portion of these contacts were in the left supramarginal gyrus. The electrode recordings exhibiting significant stimulus-induced responses in high gamma and beta band were tabulated. Each recording site was categorized as having either a positive or negative induced response, in high gamma and beta separately. If an electrode recording exhibited both positive and negative stimulus-induced responses, its site was categorized based on the earlier response. If two recordings from the same site exhibited the same response type, its site was counted only once. Two-sample t-tests were used to compare the Talairach space *x*, *y,* and *z* coordinates between sites exhibiting positive responses, to those exhibiting negative responses.

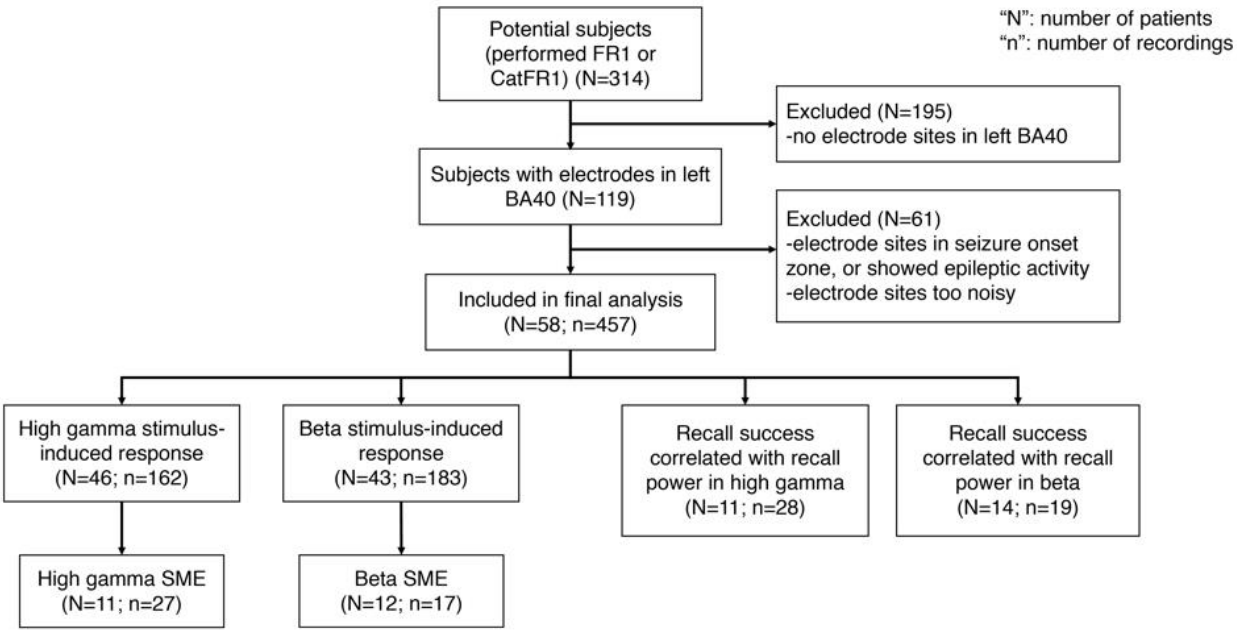

Figure 1: STAR-D diagram patient enrollment and analysis

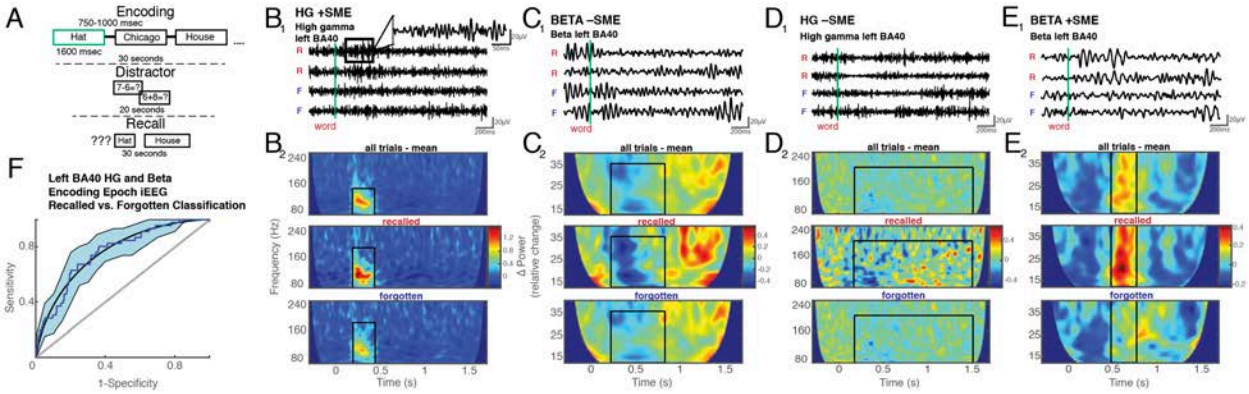

Figure 2. High-gamma and beta oscillations in left Brodmann area 40 during encoding exhibit a subsequent memory effect and predict successful recall. A) Illustration of the free recall verbal episodic memory task. B-E) Bandpass filtered iEEG recordings from left Brodmann area 40 during the encoding epoch show stimulis-induced changes in high-gamma (B1,D1) and beta band (C1,E1). Positive subsequent memory effect (SME) were evident when comparing high-gamma (B1) or beta (E1) activity during word trials that were recalled [R] to those forgotten [F]. Negative SMEs were also observed in certain electrode sites in high-gamma (D1) and beta band (C1). B2-E2 demonstrate the mean wavelet convolution of all trials, recalled trials, and forgotten trials, for each SME type, for example patients. The black boxes indicate regions in which the cluster-based comparisons exhibited a significant effect. F) Receiver operating curve with 95% confidence interval for classifying recall on the basis of high-gamma and beta band power in left Brodmann area 40 from a single patient.

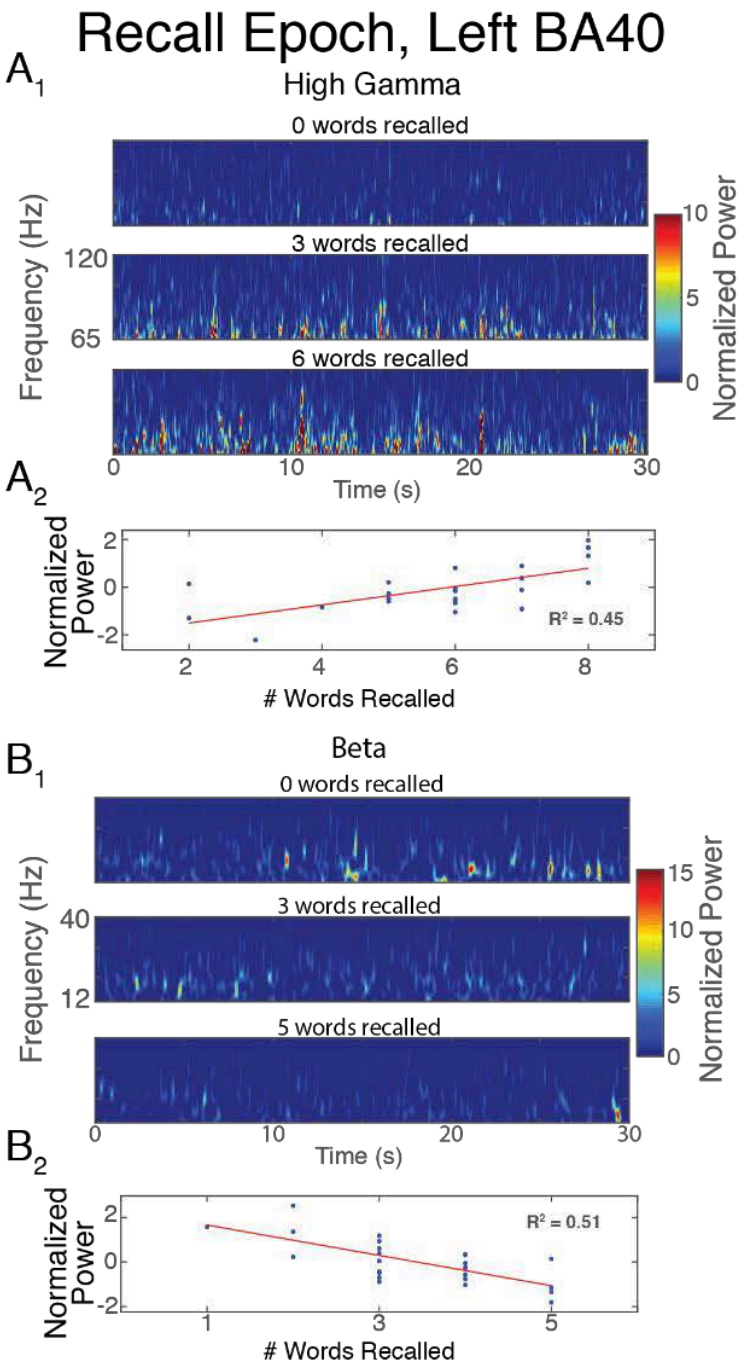

Figure 3: **High-gamma and beta oscillations during the recall epoch correlate with the number of words recalled.** A1. Wavelet convolution of high-gamma power during recall epoch recordings from a single left BA40 electrode. Note that during recall epochs in which more words were recalled both the number and the power of high-gamma bursts were increased relative to blocks with less words recalled. A2. Linear regression of normalized high-gamma power in a single left BA40 electrode and the number of words recalled. B1. Wavelet convolution of beta power during the recall epoch showing that when more word were recalled fewer beta oscillations were evident and these oscillations had less power. B2. Linear regression of beta power and the number of words recalled.

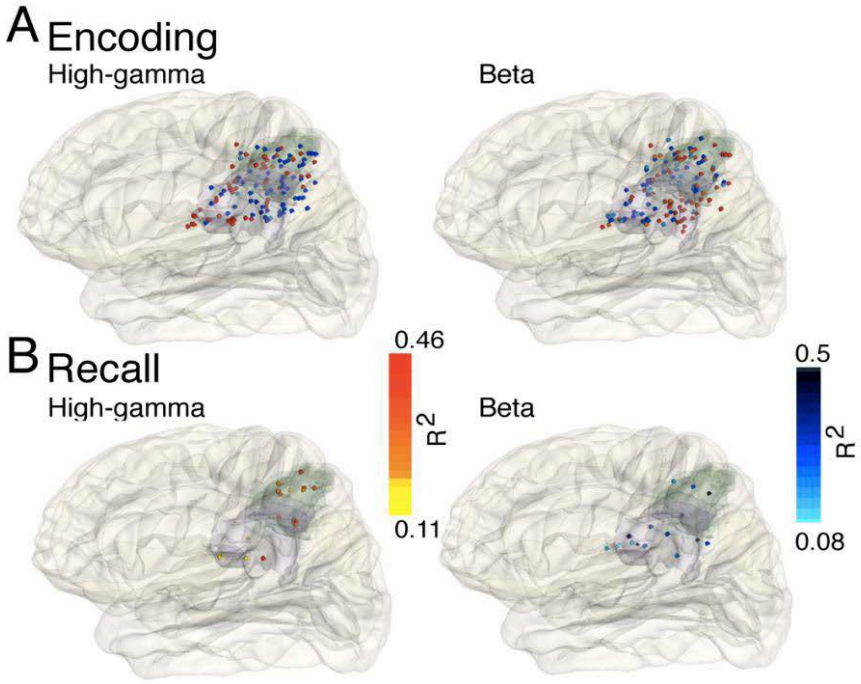

Figure 4: **Spatial distribution of attention to memory related high-gamma and beta oscillations:** A) High-gamma and beta responses elicited by visual displayof words during encoding. Red spheres indicate electrode sites wherein a statistically significant positive response was elicited, orange spheres a positive followed by negative response, blue spheres a negative response, and cyan spheres a negative followed by positive response. Purple region corresponds to left Brodmann area 40, and green region to the supramarginal gyrus. B) Coefficient of determination R^2 for the significant correlation between high-gamma activity (left) and beta activity (right) during recall epochs and the number of words recalled during the recall epoch.

Supplemental Materials

High gamma and beta band oscillations in left ventral posterior parietal cortex are regionally dissociated during verbal episodic encoding and recall

Rubinstein D[1], Camarillo-Rodriguez L[1], Waldman ZJ[1], Orosz I[5], Stein J[6], Das S[5], Gorniak R[3], Sharan AD[4], Gross R[9], Lega BC[10], Zaghloul K[11], Jobst BC[12], Davis K[9], Wanda PA[8], Worrell G, Sperling MR[2], Weiss SA[1]

Depts. of Neurology and Neuroscience,[1] [2]Dept. of Neurology, [3]Dept. of Radiology, [4]Dept. of Neurosurgery, Thomas Jefferson University, Philadelphia, PA, U.S.A. 19107. Dept. of Neurology David Geffen School of Medicine at UCLA, Los Angeles, CA, U.S.A. 90095. [7]Penn Image Computing and Science Laboratory, Department of Radiology, Department of Psychology, [9]Department of Neurology, University of Pennsylvania, Philadelphia, PA 19104, USA. [9]Department of Neurosurgery, Emory University, Atlanta GA, USA. [10]University of Texas Southwestern Medical Center, Department of Neurosurgery, Dallas TX, USA. 75390. [11]Surgical Neurology Branch, NINDS, NIH, Bethesda, MD 20892, USA. [12]Dartmouth-Hitchcock Medical Center, Department of Neurology, Lebanon NH, USA. 03756.

Supplementary Table 1. Demographic and clinical information for patients included in left Brodmann area 40 analysis.

Subject ID	Age	Gender	Handedness	Dominant hemisphere	Verbal Comprehension Index (WAIS IV)	MRI abnormalities	Seizure Onset Zone	Tasks	Recall rate
R1003	39	Female	Ambidextrous	Left	107	None	L anterior temporal	FR1	0.33
R1021	39	Male	Right	Left	74	None	L temporal, parietal, R mesial temporal	CatFR1	0.29
R1022	25	Male	Right	Left	81	Atrophy/tissue loss, Encephaloma/gliosis	L cingulate	FR1	0.27
R1026	25	Female	Right	Undetermined	112	Mesial temporal sclerosis, Encephaloma/gliosis	L anterior temporal; rare L occipital/suboccipital	CatFR1/FR1	0.33/0.23
R1036	49	Male	Left	Right		Mesial temporal sclerosis, Encephaloma/gliosis	L anterior and mesial temporal	FR1	0.16
R1049	52	Female	Right	Left	95	Atrophy/tissue loss, Encephaloma/gliosis	L anterior to mid hippocampal	FR1	0.08
R1052	20	Female	Right	Undetermined		None	R cingulate	FR1	0.28
R1059	45	Female	Right	Left	70	None	Bilateral temporal	FR1	0.08
R1065	34	Female	Right	Undetermined	116	None	Bilateral temporal	CatFR1/FR1	0.65/0.34
R1067	45	Female	Right	Left		Other	L anterior and inferior temporal	CatFR1/FR1	0.20/0.17
R1069	27	Male	Right	Left		Malformation of cortical development	L anterior lateral frontal, L parietal	CatFR1/FR1	0.49/0.29
R1070	40	Female	Right	Left		Other	L mesial temporal, occipital	FR1	0.16
R1074	25	Male	Right	Undetermined		None	Undetermined	CatFR1/FR1	0.27/0.19
R1080	43	Female	Right	Undetermined	91	None	R mesial temporal, L temporal	FR1	0.28
R1084	25	Male	Right	Left		None	L medial primary sensory cortex	FR1	0.18
R1086	21	Male	Left	Left		None	L anterior temporal	CatFR1/FR1	0.12/0.3
R1094	47	Male	Right	Left		None	L mesial temporal, parietal	CatFR1/FR1	0.12
R1100	44	Female	Right	Left	103	None	L mesial temporal	FR1	0.03
R1101	26	Female	Left	Right		Mesial temporal sclerosis, Encephaloma/gliosis	L mesial temporal	FR1	0.22
R1102	35	Male	Right	Left		Atrophy/tissue loss	Bilateral mesial temporal	CatFR1/FR1	0.32/0.25
R1107	25	Male	Right	Undetermined	100	Other	L occipital	CatFR1	0.57
R1111	20	Male	Right	Left		Encephaloma/gliosis	L anterior temporal, parietal/occipital	CatFR1/FR1	0.58/0.54
R1114	32	Female	Ambidextrous	Undetermined	110	None	L posterior temporal, parietal	CatFR1/FR1	0.42/0.24
R1118	33	Male	Right	Undetermined	98	Malformation of cortical development	L posterior subtemporal	FR1	0.18
R1120	34	Female	Left	Undetermined	93	None	R mesial temporal	FR1	0.35
R1125	45	Female	Right	Left		None	Undetermined	FR1	0.20
R1130	57	Male	Right	Left		Encephaloma/gliosis	L mesial and lateral superior frontal	CatFR1/FR1	0.28/0.20

R1134	65	Male	Right	Left		Encephaloma/gliosis	L occipital, bilateral mesial temporal	FR1	0.09
R1135	48	Male	Right	Left	78	Other	L inferior parieto-occipital	CatFR1/FR1	0.14/0.09
R1138	42	Male	Right	Left		Mesial temporal sclerosis	L mesial temporal, R parietal	CatFR1/FR1	0.19/0.17
R1153	38	Male	Left	Left		Mesial temporal sclerosis	L anterior hippocampus, R mesial temporal	FR1	0.12
R1177	23	Female	Right	Left		Other	L posterior temporal	FR1	0.24
R1221	57	Male	Right	Left	87	Other	L mesial temporal, temporal, limbic	CatFR1/FR1	0.28/0.3
R1266	48	Female	Left	Undetermined	76	Mesial temporal sclerosis, Encephaloma/gliosis	L mesial temporal	CatFR1	0.152
R1286	58	Female	Right	Undetermined	127	Vascular, Neoplasm, Other	L limbic, parietal, insular	CatFR1/FR1	0.24/0.25
R1291	35	Male	Right	Left		Other	L temporal, frontal, temporal/occipital	CatFR1/FR1	0.54/0.36
R1297	25	Male	Right	Left	100	Malformation of cortical development	L mesial/middle temporal, R temporal	FR1	0.27
R1310	20	Male	Right	Undetermined	103	Other	L temporal	CatFR1	0.42
R1317	36	Male	Right	Undetermined	93	Other	L mesial temporal	CatFR1/FR1	0.38/0.23
R1323	40	Male	Right	Left		None	Bilateral mesial temporal	FR1	0.22
R1330	38	Female	Right	Undetermined	122	Other	Bilateral cingulate	CatFR1/FR1	0.38/0.31
R1338	22	Male	Left	Left		Other	R parietal	CatFR1	0.14
R1339	29	Male	Left	Undetermined	105	Other	Undetermined	FR1	0.18
R1345	48	Male	Ambidextrous	Undetermined	81	Other	Undetermined	FR1	0.19
R1346	38	Female	Right	Left		None	Bilateral temporal	FR1	0.21
R1348	43	Male	Right	Left	81	None	L temporo-occipital	CatFR1	0.17
R1355	37	Male	Left	Undetermined		Encephaloma/gliosis	L mesial temporal	FR1	0.09
R1358	35	Male	Right	Left		Other	L temporal, parietal	FR1	0.21
R1372	49	Female	Right	Undetermined		Other	Undetermined	CatFR1	0.21
R1373	32	Female	Right	Left		Other	L insular/frontal	FR1	0.19
R1378	39	Male	Right	Left		Atrophy/tissue loss	L frontal	CatFR1/FR1	0.42/0.29
R1379	50	Male	Right	Undetermined	83	None	L temporal	CatFR1/FR1	0.22/0.18
R1384	25	Male	Left	Undetermined	98	None	R cingulate/frontal	CatFR1/FR1	0.34/0.20
R1386	55	Female	Right	Left		None	R mesial temporal, temporal/occipital	CatFR1/FR1	0.29/0.24
R1390	32	Male	Right	Left	103	Malformation of cortical development	L temporal/parietal	FR1	0.21
R1398	45	Male	Right	Undetermined	105	Other	Undetermined	CatFR1/FR1	0.37/0.22
R1421	58	Female	Ambidextrous	Left	114	Other	Undetermined	CatFR1/FR1	0.14/0.16
X082	57	Female	Right	Left		None	L mesial temporal	FR1	0.23

Supplementary Table 3. Demographic information for patients included in analyses for left Brodmann area 21, left entorhinal cortex (Brodmann areas 28 and 34), and right Brodmann area 40.

Subject ID	Age	Gender	Handedness	Dominant hemisphere	Tasks	Recall rate	Site
R1001	48	Female	Right	Left	FR1	0.19	RBA40
R1003	39	Female	Ambidextrous	Left	FR1	0.33	LBA21, LBA28/34
R1004	52	Female	Right	Undetermined	CatFR1	0.04	LBA28/34
R1010	31	Female	Ambidextrous	Left	FR1	0.19	RBA40
R1013	37	Female	Right	Left	CatFR1	0.27	LBA28/34
R1015	55	Female	Left	Left	FR1	0.17	LBA28/34, RBA40
R1021	39	Male	Right	Left	CatFR1	0.29	LBA21, RBA40
R1022	25	Male	Right	Left	FR1	0.27	LBA21
R1029	33	Female	Right	Undetermined	CatFR1	0.28	LBA21
R1032	20	Female	Right	Left	CatFR1/FR1	0.28/0.32	RBA40
R1033	32	Female	Right	Left	FR1	0.21	LBA28/34, RBA40
R1036	49	Male	Left	Right	FR1	0.16	LBA21, LBA28/34
R1044	59	Male	Right	Undetermined	CatFR1/FR1	0.19/0.19	LBA28/34, RBA40
R1045	51	Male	Right	Left	CatFR1/FR1	0.41/0.33	LBA28/34
R1049	52	Female	Right	Left	FR1	0.08	LBA21, LBA28/34
R1052	20	Female	Right	Undetermined	FR1	0.28	LBA28/34
R1059	45	Female	Right	Left	FR1	0.08	LBA21, LBA28/34, RBA40
R1063	24	Male	Right	Undetermined	FR1	0.23	LBA28/34, RBA40
R1065	34	Female	Right	Undetermined	CatFR1/FR1	0.65/0.34	LBA21, LBA28/34, RBA40
R1066	39	Male	Right	Left	CatFR1/FR1	.26/0.31	LBA28/34
R1067	45	Female	Right	Left	CatFR1/FR1	0.20/0.17	LBA28/34
R1070	40	Female	Right	Left	FR1	0.16	LBA21
R1077	48	Female	Right	Undetermined	FR1	0.3	LBA28/34, RBA40
R1080	43	Female	Right	Undetermined	FR1	0.28	LBA21
R1083	49	Female	Right	Left	FR1	0.22	LBA21
R1086	21	Male	Left	Left	CatFR1/FR1	0.12/0.30	LBA21
R1089	36	Male	Left	Left	CatFR1/FR1	0.17/0.16	LBA28/34, RBA40

R1092	45	Male	Right	Left	CatFR1/FR1	0.31/0.23	RBA40
R1094	47	Male	Right	Left	CatFR1/FR1	0.12/0.12	LBA21
R1100	44	Female	Right	Left	FR1	0.03	LBA21
R1101	26	Female	Left	Right	FR1	0.22	LBA21
R1102	35	Male	Right	Left	CatFR1/FR1	0.32/0.25	LBA21
R1107	25	Male	Right	Undetermined	CatFR1	0.57	LBA21
R1108	24	Female	Right	Right	CatFR1/FR1	0.42/0.23	RBA40
R1111	20	Male	Right	Left	CatFR1/FR1	0.58/0.54	LBA21
R1113	37	Female	Right	Left	FR1	0.34	LBA28/34, RBA40
R1114	32	Female	Ambidextrous	Undetermined	CatFR1/FR1	0.42/0.24	LBA21
R1118	33	Male	Right	Undetermined	FR1	0.18	LBA21
R1119	27	Female	Left	Right	CatFR1	0.09	LBA21
R1120	34	Female	Left	Undetermined	FR1	0.35	LBA21, RBA40
R1125	45	Female	Right	Left	FR1	0.2	LBA21
R1134	65	Male	Right	Left	FR1	0.09	LBA21
R1135	48	Male	Right	Left	CatFR1/FR1	0.14/0.09	LBA21, LBA28/34, RBA40
R1136	57	Female	Right	Undetermined	FR1	0.2	LBA21
R1138	42	Male	Right	Left	FR1	0.19/0.17	LBA21, RBA40
R1147	48	Male	Right	Left	CatFR1	0.2	LBA21
R1153	38	Male	Left	Left	FR1	0.12	LBA21, RBA40
R1154	36	Female	Right	Left	FR1	0.3	LBA28/34
R1159	43	Female	Right	Left	FR1	0.24	RBA40
R1168	24	Male	Right	Left	FR1	0.29	LBA28/34, RBA40
R1171	36	Male	Right	Undetermined	CatFR1/FR1	0.27/0.25	LBA28/34, RBA40
R1175	34	Male	Right	Undetermined	FR1	0.23	LBA28/34
R1177	23	Female	Right	Left	FR1	0.24	LBA21
R1180	21	Female	Right	Left	CatFR1	0.35	LBA28/34
R1185	21	Male	Right	Undetermined	FR1	0.33	LBA28/34
R1186	28	Male	Undetermined	Undetermined	CatFR1/FR1	0.11/0.08	RBA40
R1190	58	Female	Right	Left	CatFR1	0.16	LBA21
R1195	44	Male	Right	Left	FR1	0.3	RBA40
R1203	36	Female	Right	Left	FR1	0.18	LBA28/34, RBA40

R1217	37	Male	Right	Left	CatFR1/FR1	0.44/0.25	LBA28/34, RBA40
R1221	57	Male	Right	Left	CatFR1/FR1	0.28/0.30	LBA21
R1226	42	Female	Right	Undetermined	FR1	0.26	LBA21, LBA28/34
R1228	59	Female	Right	Undetermined	CatFR1/FR1	0.29/0.27	LBA28/34
R1236	52	Female	Right	Left	CatFR1/FR1	0.50/0.26	LBA28/34
R1239	27	Male	Right	Left	CatFR1	0.3	LBA28/34
R1241	52	Male	Right	Left	FR1	0.09	LBA28/34, RBA40
R1247	62	Female	Right	Undetermined	CatFR1/FR1	0.23/0.31	LBA28/34
R1260	57	Female	Right	Undetermined	FR1	0.25	LBA21
R1273	48	Female	Left	Undetermined	CatFR1	0.16	LBA21, LBA28/34
R1278	22	Female	Right	Left	CatFR1	0.27	LBA28/34, RBA40
R1311	22	Male	Right	Left	FR1	0.19	LBA28/34
X082	57	Female	Right	Left	FR1	0.23	LBA21, LBA28/34

Supplementary Table 3. Attributes of recall performance classifier for left Brodmann area 40.

Subject ID	Experiment	Total number of LBA40 electrodes	Number of electrodes used (with significant response)	Number of trials	AUROC
R1003	FR1	1	1	564	0.68
R1036	FR1	6	4	300	0.62
R1069	CatFR1	11	3	300	0.66
R1069	FR1	11	5	300	0.67
R1084	FR1	30	11	180	0.66
R1094	FR1	13	12	900	0.76
R1094	CatFR1	13	12	300	0.75
R1102	CatFR1	2	2	360	0.71
R1107	CatFR1	2	2	540	0.59
R1114	FR1	7	6	300	0.61
R1134	FR1	6	3	840	0.64
R1138	CatFR1	6	3	720	0.61
R1221	CatFR1	5	5	900	0.57
R1221	FR1	5	4	300	0.6
R1286	FR1	4	3	300	0.72
R1291	CatFR1	9	5	600	0.57
R1310	CatFR1	5	5	600	0.72
R1317	CatFR1	12	7	300	0.7
R1323	FR1	12	7	840	0.56
R1346	FR1	5	4	900	0.63
R1378	FR1	7	3	576	0.65
R1378	CatFR1	7	6	288	0.62

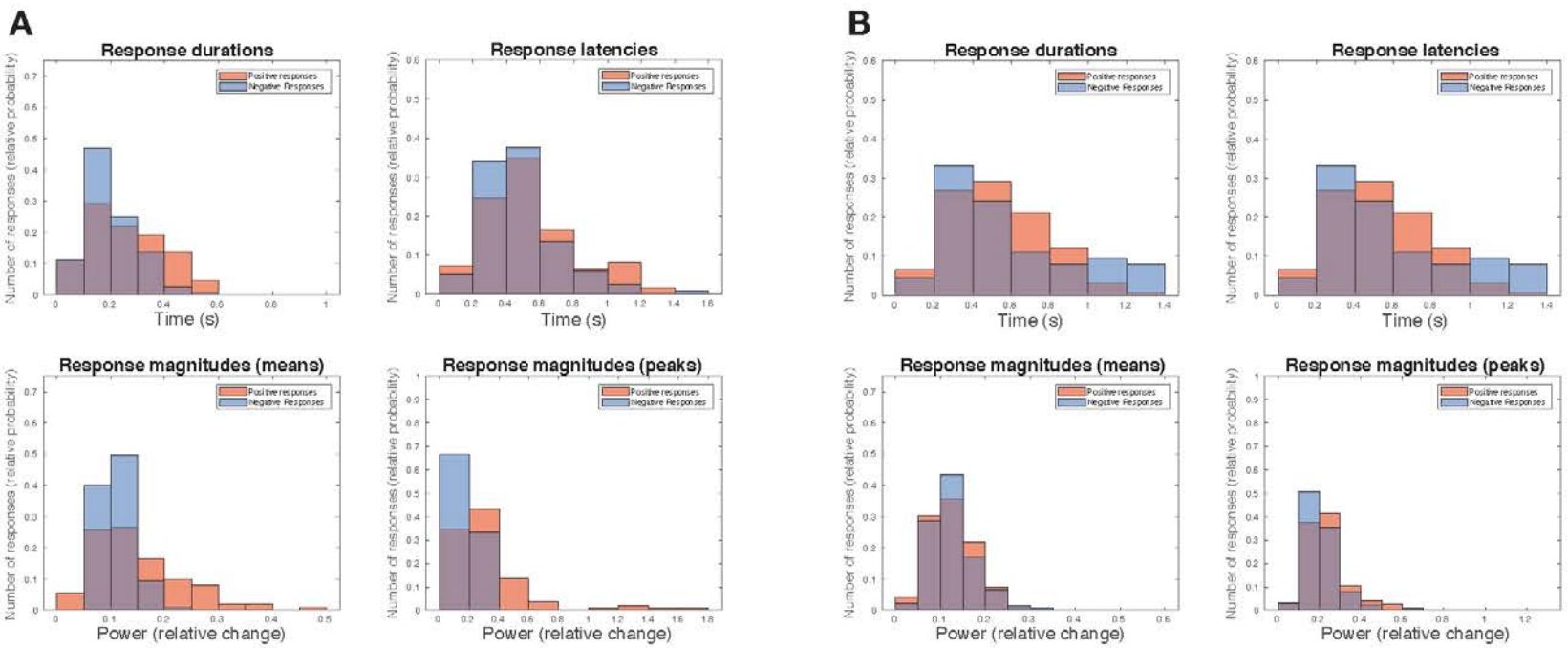

Supplementary Figure 1. Characteristics of high gamma and beta induced responses in left Brodmann area 40 during encoding. Response durations, latencies (at peak t-statistic), mean magnitudes, and peak magnitudes of significant high gamma (A) and beta band (B) induced responses. Positive induced responses shown in red, negative responses shown in blue.

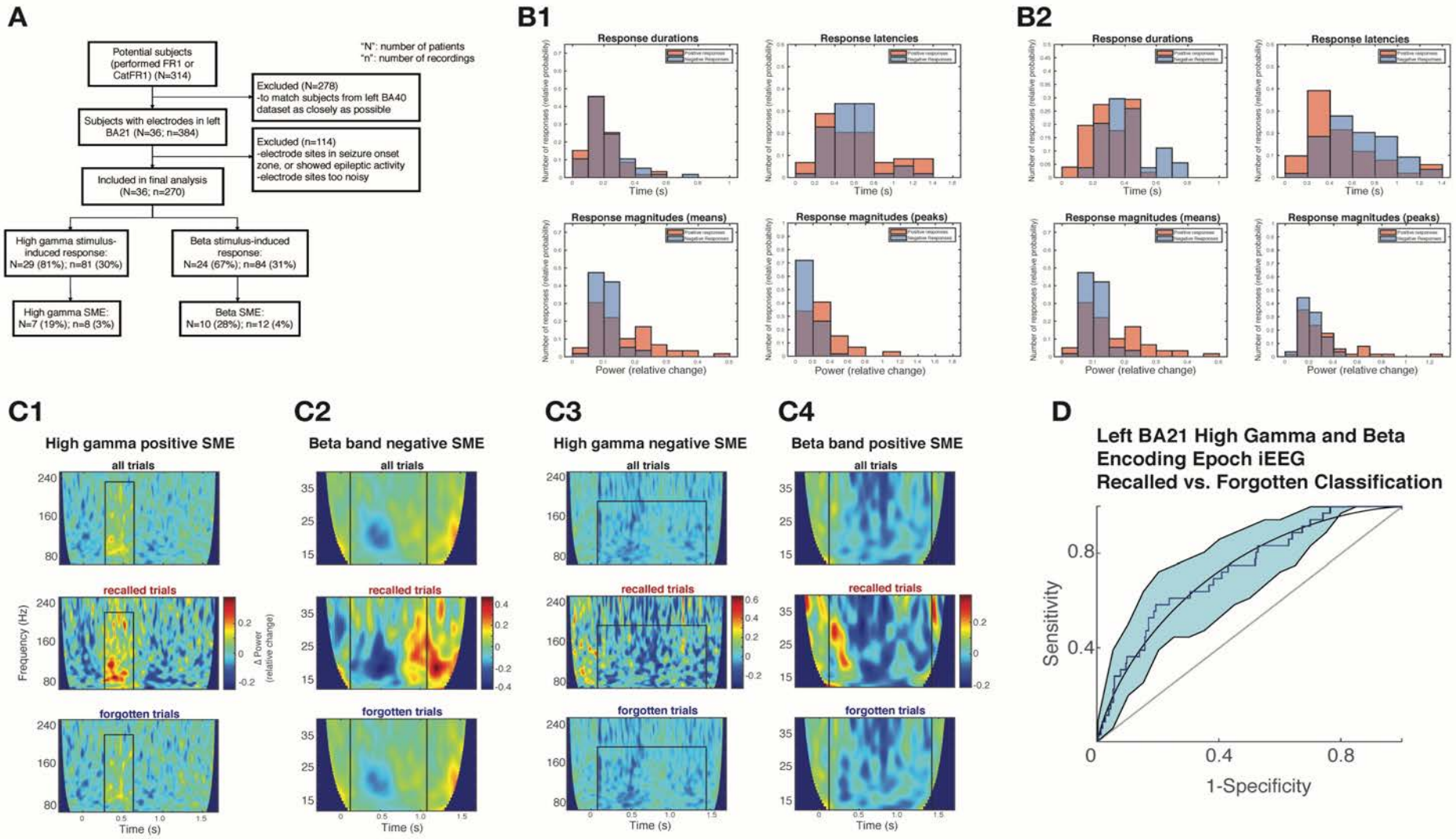

Supplementary Figure 2. Characteristics of high gamma and beta induced responses in left Brodmann area 21 during encoding. A) STAR-D diagram of patient enrollment and analysis. B) Response durations, latencies (at peak t-statistic), mean magnitudes, and peak magnitudes of significant high gamma (B1) and beta band (B2) induced responses. Positive induced responses shown in red, negative responses shown in blue. C) Mean wavelet convolutions of all trials, recalled trials, and forgotten trials, for example electrode recordings exhibiting a positive high gamma SME (C1), and negative beta band SME (C2), a negative high gamma SME (C3), and a positive beta band SME (C4). D) Receiver operating curve with 95% confidence interval for classifying recall on the basis of high gamma and beta band power in left Brodmann area 21 in a single patient.

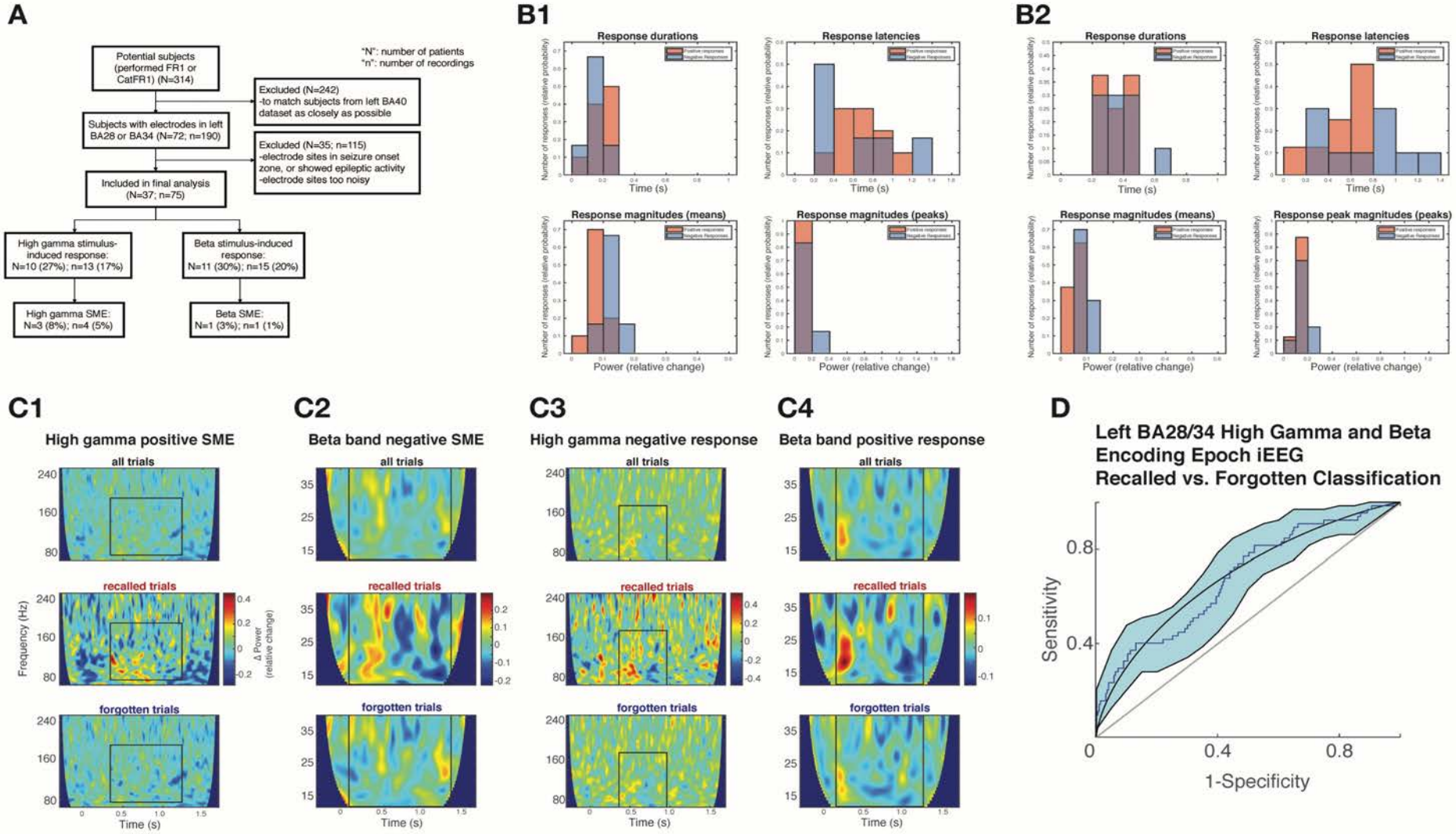

Supplementary Figure 3. Characteristics of high gamma and beta induced responses in left Brodmann areas 28 and 34 during encoding. A) STAR-D diagram of patient enrollment and analysis. B) Response durations, latencies (at peak t-statistic), mean magnitudes, and peak magnitudes of significant high gamma (B1) and beta band (B2) induced responses. Positive induced responses shown in red, negative responses shown in blue. C) Mean wavelet convolutions of all trials, recalled trials, and forgotten trials, for example electrode recordings exhibiting a positive high gamma SME (C1), and negative beta band SME (C2), a negative high gamma induced response (C3), and a positive beta band induced response (C4). D) Receiver operating curve with 95% confidence interval for classifying recall on the basis of high gamma and beta band power in left Brodmann areas 28 and 34 in a single patient.

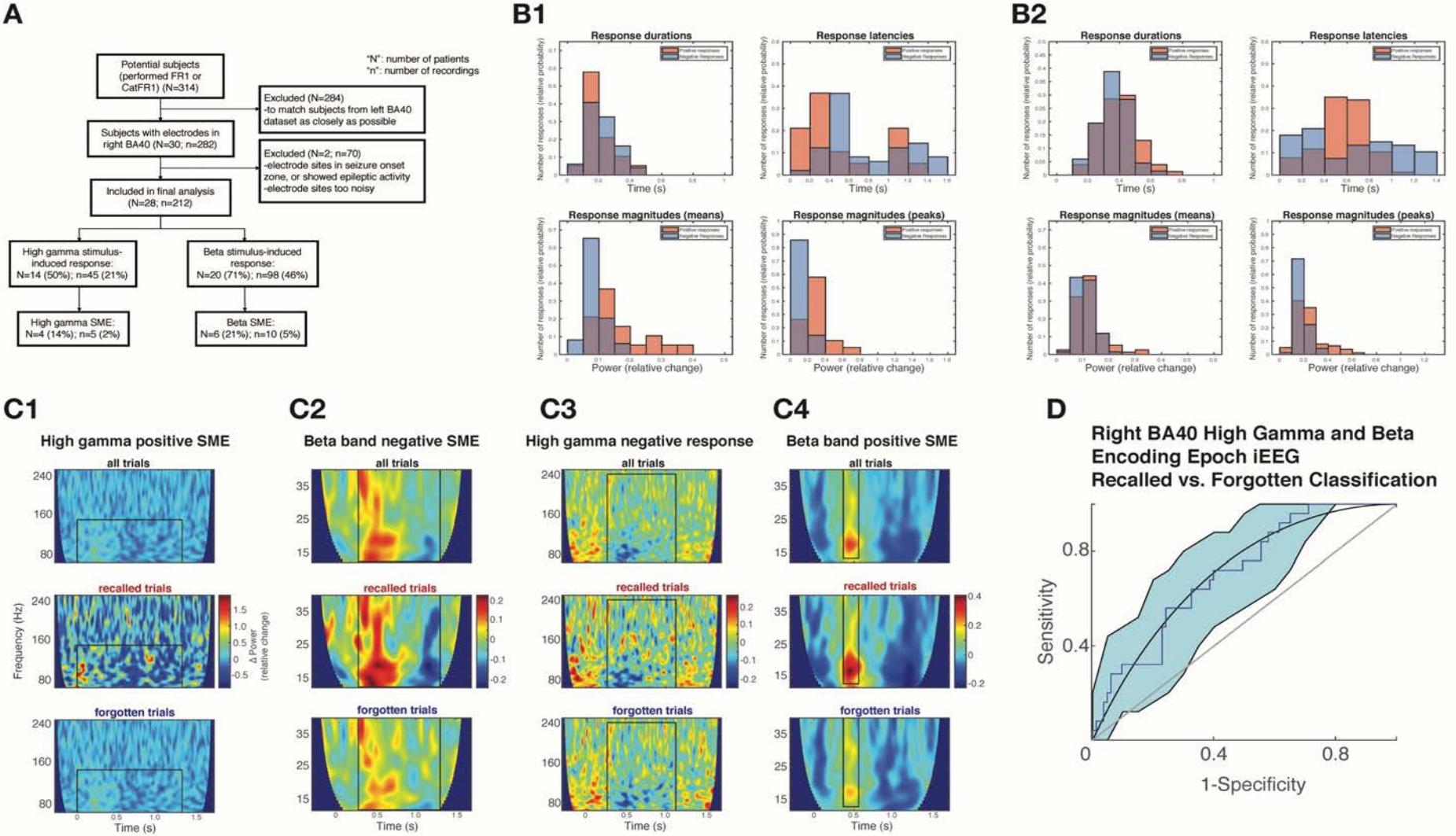

Supplementary Figure 4. Characteristics of high gamma and beta induced responses in right Brodmann area 40. A) STAR-D diagram of patient enrollment and analysis. B) Response durations, latencies (at peak t-statistic), mean magnitudes, and peak magnitudes of significant high gamma (B1) and beta band (B2) induced responses. Positive induced responses shown in red, negative responses shown in blue. C) Mean wavelet convolutions of all trials, recalled trials, and forgotten trials, for example electrode recordings exhibiting a positive high gamma SME (C1), and negative beta band SME (C2), a negative high gamma induced response (C3), and a positive beta band SME (C4). D) Receiver operating curve with 95% confidence interval for classifying recall on the basis of high gamma and beta band power in right Brodmann area 40 in a single patient.

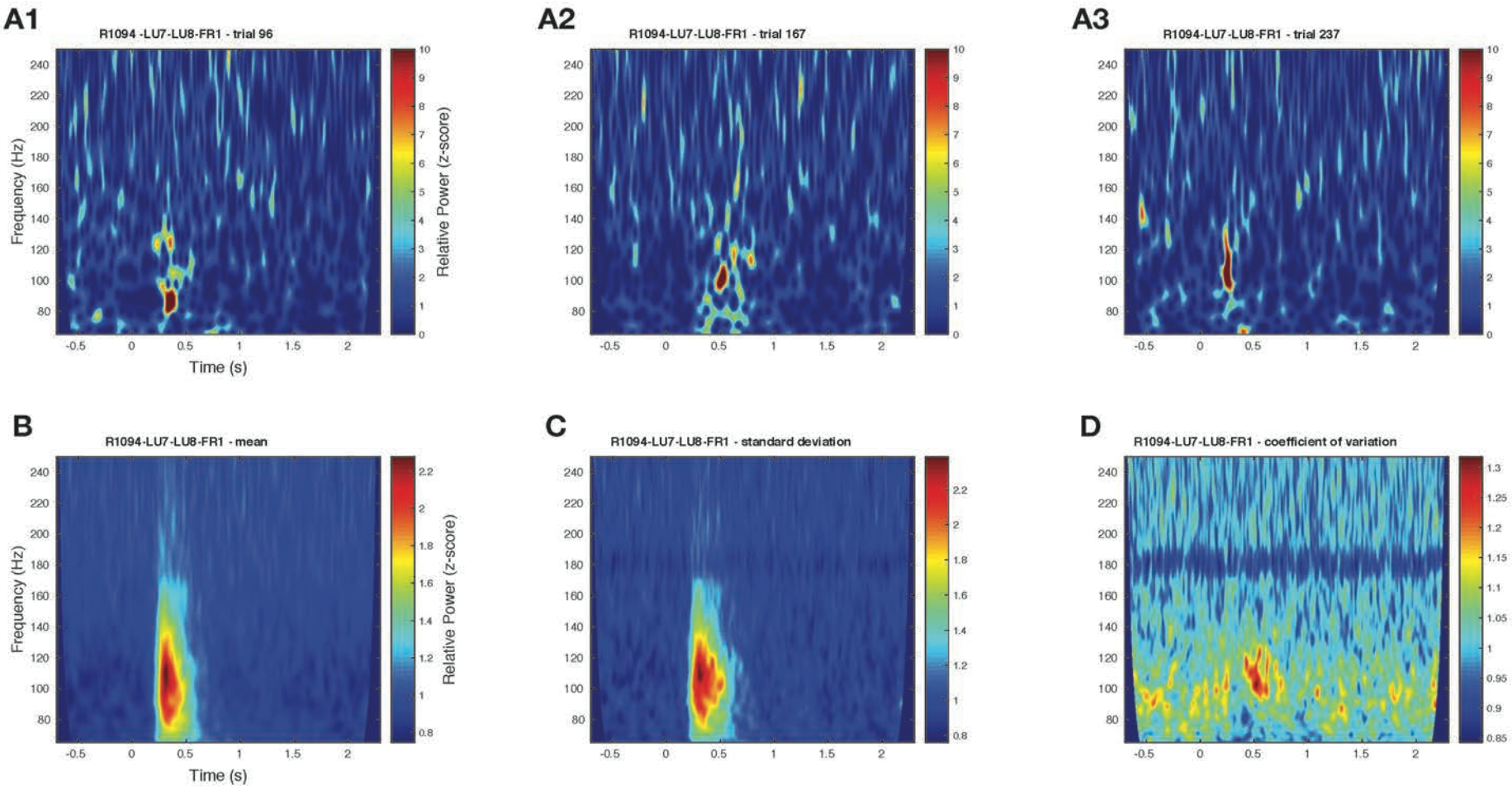

Supplementary Figure 5. Example single trials and summary plots of high gamma induced responses in left Brodmann area 40.
A) Examples of single trials from one electrode from one patient. B-D) Mean (B), standard deviation (C) and coefficient of variation (D) of all trials (recalled and forgotten) for the same electrode recording. Single trial examples demonstrate that the mean response is not an artifact of trial averaging, nor an artifact of very few individual responses, but rather resembles many individual responses. This is further illustrated in the coefficient of variation, which shows that the greatest relative variability lies not in the center of the mean response, but rather at the trailing edge, just after 0.5s post-stimulus. The band of reduced relatively variability at 180Hz likely reflects the powerline filter.

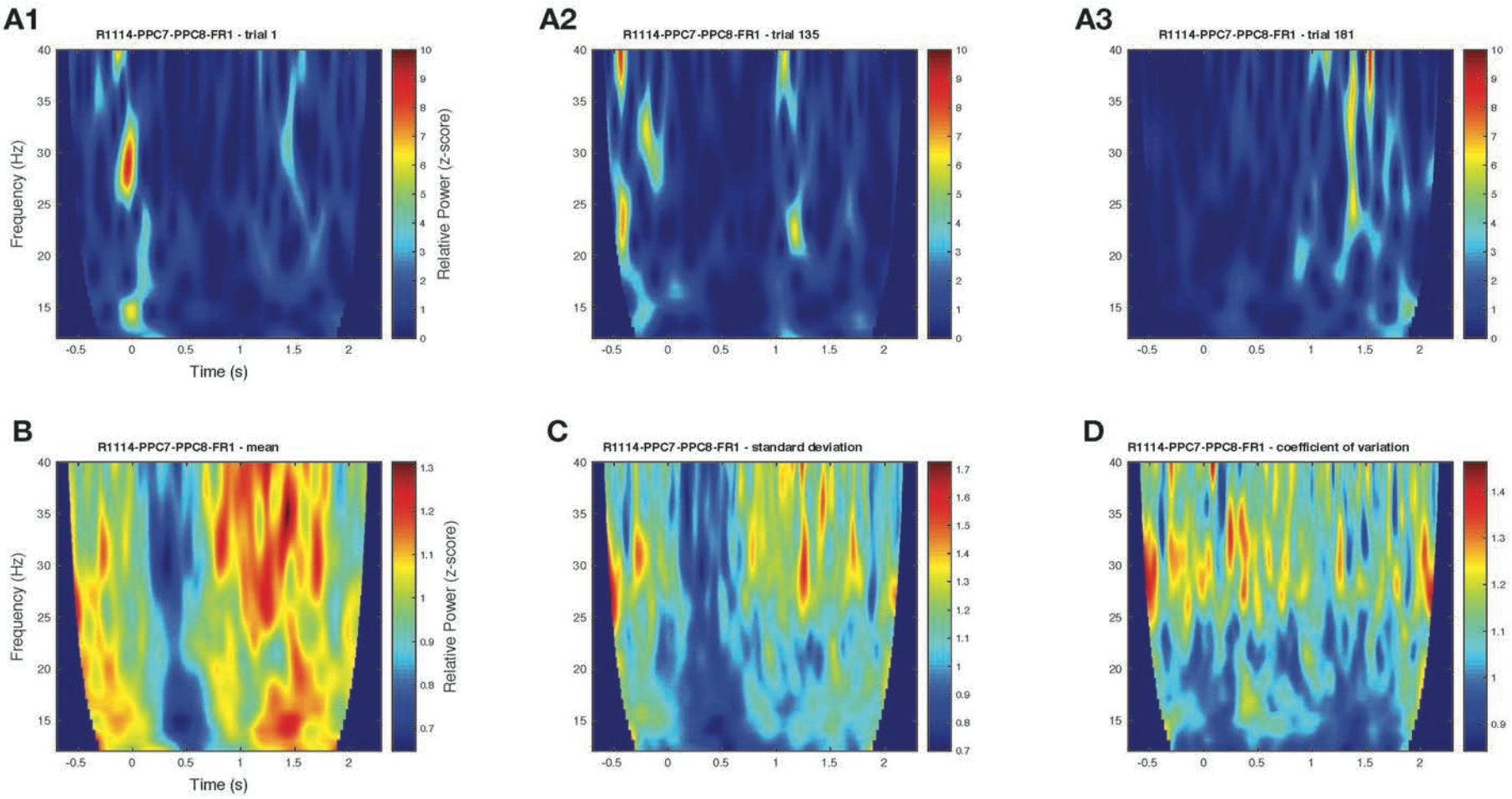

Supplementary Figure 6. Example single trials and summary plots of beta band induced responses in left Brodmann area 40. A) Examples of single trials from one electrode from one patient. B-D) Mean (B), standard deviation (C) and coefficient of variation (D) of all trials (recalled and forgotten) for the same electrode recording. Unlike the high gamma response, there is not a distinct positive beta band response in this electrode. Rather, here is demonstrated the significantly reduced probability of beta activity around 0.5s post-stimulus, which can be seen even in individual trials.

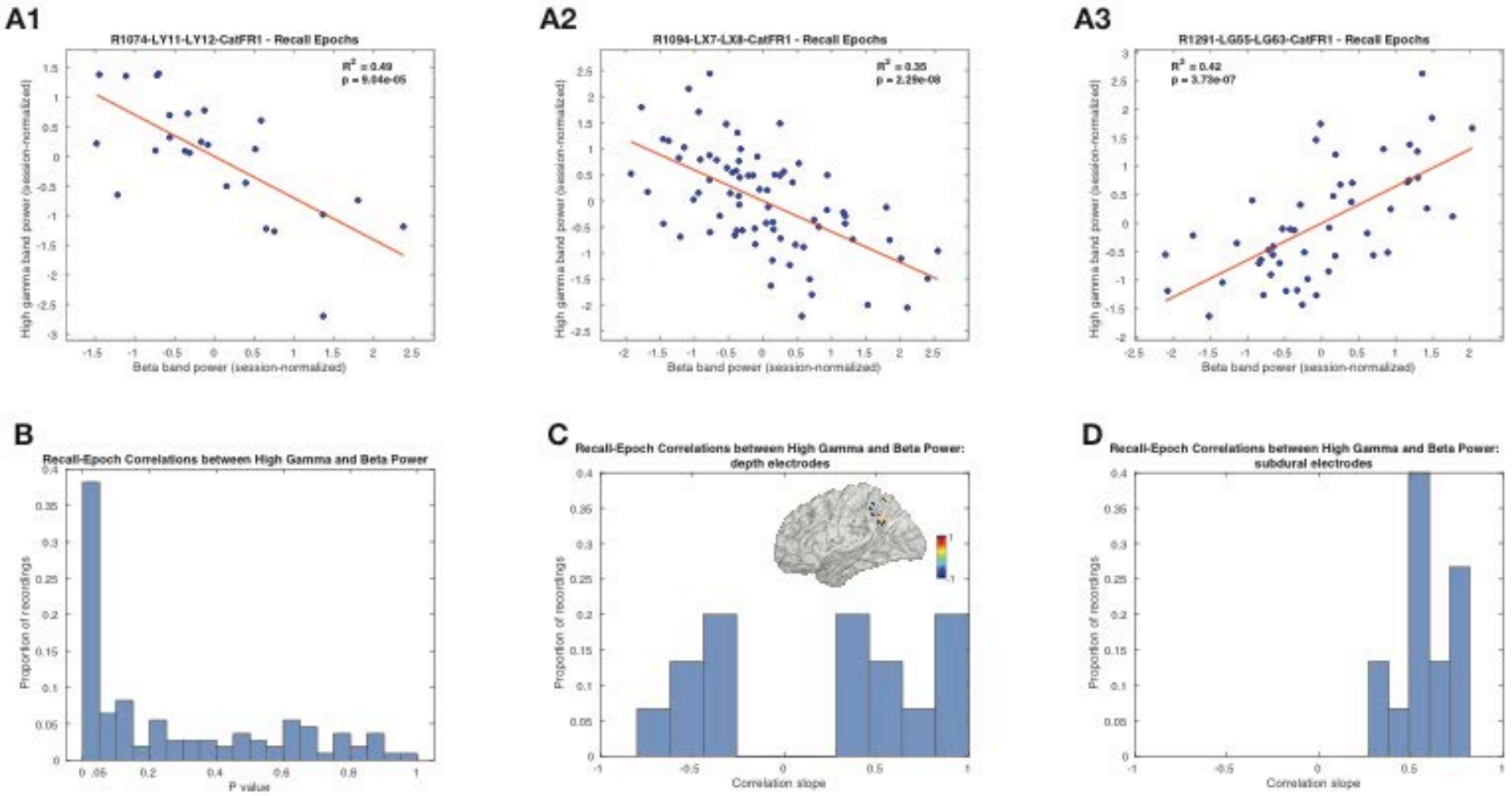

Supplementary Figure 7. Correlation between high gamma and beta band power during recall epochs in left Brodmann area 40. A) Examples from single electrodes from individual patients. B) Distribution of p-values for electrodes showing significant ($p<0.05$, uncorrected) correlation of recall number and either high gamma or beta band power during the recall epoch. C-D) Distribution of slopes of significant ($p<0.05$, FDR corrected) correlations between high gamma and beta band power during recall epoch, for depth electrodes (C) or subdural electrodes (D). Inset in (C) shows spatial locations of electrodes; those with negative correlations were significantly anterior to those with positive correlations ($p<0.01$). Note that while correlations between high gamma and beta band power from depth electrodes are not significantly different from 0 overall ($p>0.2$), from subdural electrodes, all correlations are positive.

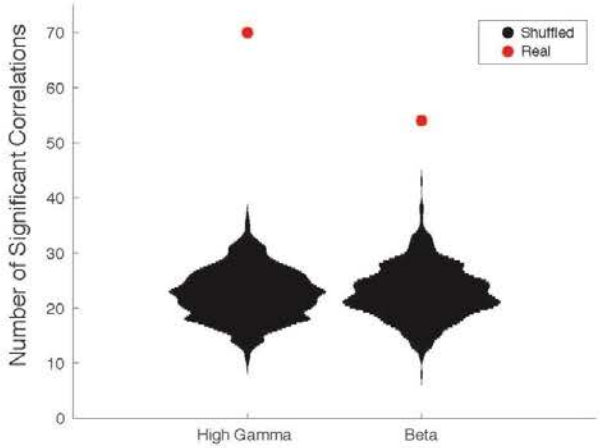

Supplementary Figure 8. Number of correlations between recall number and recall-epoch band-power in 1000 random shuffles. Significant correlations here are $p<0.05$ uncorrected for multiple comparisons, counted over all electrode recordings and subjects. In black are the histograms of number of significant correlations for the 1000 random shuffles in each frequency band. Red dots indicate the number of significant correlations in the true arrangements.

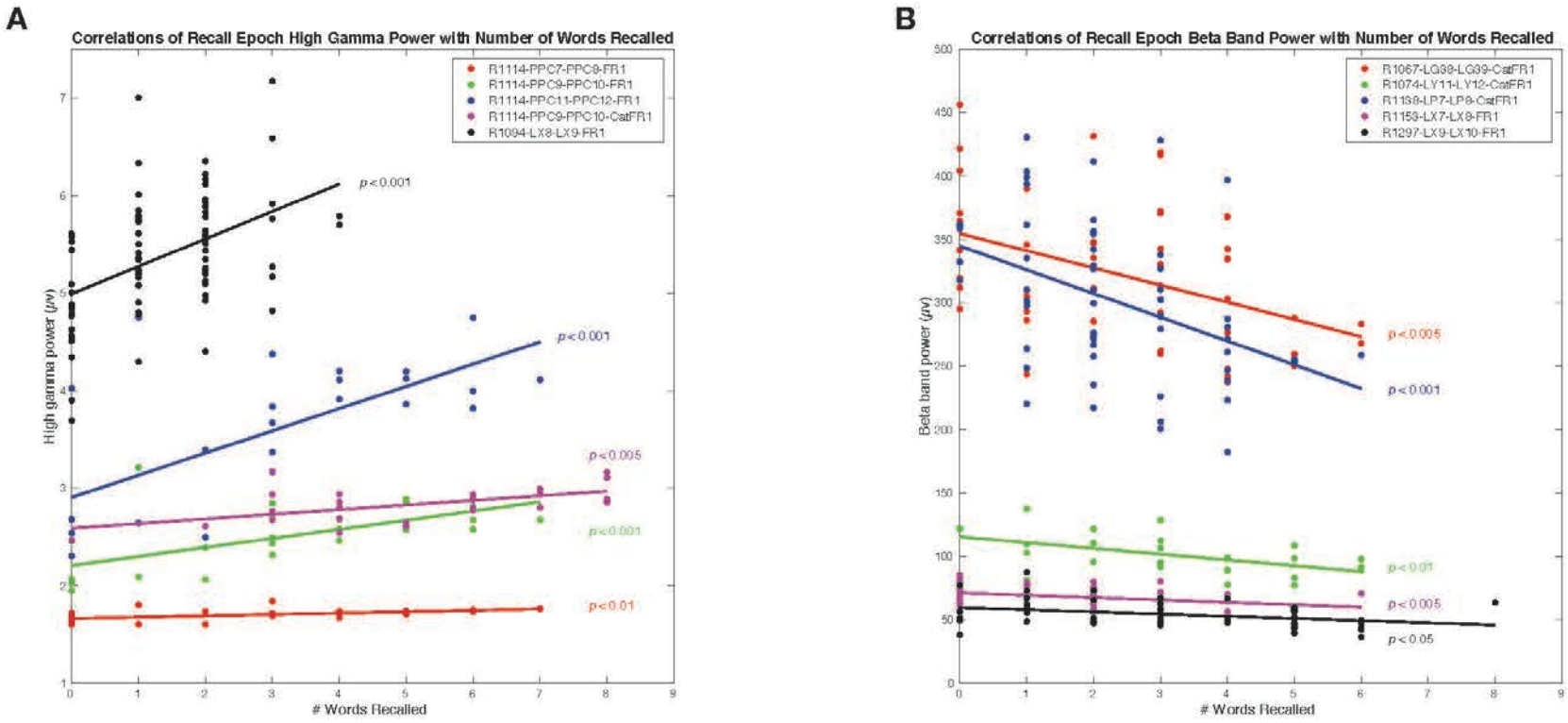

Supplementary Figure 9. Correlations between recall number and recall-epoch band power in left Brodmann area 40. Examples from single electrodes from individual patients, showing significant correlations between absolute high gamma (A) or beta band (B) power and number of words recalled. B) Subject identifier, electrode name, and task, are indicated in legend. P values of each individual correlation are indicated to the right of the plot.